Aerosol-cloud interactions at the four candidate sites of the ANAtOLIA project

S. Cavazzani, Chiara Bertolin, S. Ortolani, C. Giordano, J. Descloitres, P. Fiorentin, S. Victori, Y. Gonzalez Ramos, Abdanour Irbah, Julien Delanoë, et al.

▶ **To cite this version:**

S. Cavazzani, Chiara Bertolin, S. Ortolani, C. Giordano, J. Descloitres, et al.. Aerosol-cloud interactions at the four candidate sites of the ANAtOLIA project. RAS Techniques and Instruments, 2023, 2, pp.420-431. 10.1093/rasti/rzad030 . insu-04195451v2

HAL Id: insu-04195451
https://insu.hal.science/insu-04195451v2

Submitted on 4 Sep 2023

HAL is a multi-disciplinary open access archive for the deposit and dissemination of scientific research documents, whether they are published or not. The documents may come from teaching and research institutions in France or abroad, or from public or private research centers.

L'archive ouverte pluridisciplinaire **HAL**, est destinée au dépôt et à la diffusion de documents scientifiques de niveau recherche, publiés ou non, émanant des établissements d'enseignement et de recherche français ou étrangers, des laboratoires publics ou privés.

Distributed under a Creative Commons Attribution 4.0 International License

RAS Techniques and Instruments

RASTAI **2,** 420–431 (2023) https://doi.org/10.1093/rasti/rzad030
Advance Access publication 2023 July 18

Aerosol–cloud interactions at the four candidate sites of the ANAtOLIA project

S. Cavazzani,[1,2,3] C. Bertolin,[1★] S. Ortolani,[2,3] C. Giordano,[4] J. Descloitres,[5] P. Fiorentin,[6] S. Victori,[7] Y. Gonzalez Ramos,[8] A. Irbah,[9] J. Delanoe,[9] F. Berto[1] and A. Ziad[4]

[1]*NTNU, Department of Mechanical and Industrial Engineering, Gloshaugen, Richard Birkelands vei 2b, 7034 Trondheim, Norway*
[2]*Department of Physics and Astronomy, University of Padova, Vicolo dell'Osservatorio 3, I-35122 Padova, Italy*
[3]*INAF – Osservatorio Astronomico di Padova, Vicolo dell'Osservatorio 5, I-35122 Padova, Italy*
[4]*Université Côte d'Azur, Observatoire de la Côte d'Azur, Laboratoire Lagrange, Parc Valrose, F-06108 Nice Cedex 2, France*
[5]*AERIS/ICARE Data and Services Center, University of Lille, CNRS, CNES, UAR 2877, F-59000 Lille, France*
[6]*Department of Industrial Engineering, University of Padova, Via Gradenigo 6a, I-35131 Padova, Italy*
[7]*CIMEL Electronique, Research and Development Department, Rue de Charonne 172, F-75011 Paris, France*
[8]*Izana Atmospheric Research Centre (CIAI-AEMET), La Marina 20, P6, E-38001 Santa Cruz Tenerife, Spain*
[9]*LATMOS/IPSL, UVSQ Paris-Saclay University, Sorbonne University, CNRS, 11 BD D'Alembert Guyancourt, F-78280 Paris, France*

Accepted 2023 July 18. Received 2023 July 10; in original form 2023 February 20

ABSTRACT

ANAtOLIA (Atmospheric monitoring to Assess the availability of Optical Links through the Atmosphere) is a European Space Agency project aimed at selecting sites for optical communication in the atmosphere. The main monitored parameters are cloud cover, aerosol in relation to atmospheric turbulence aimed at monitoring and forecasting the influence of aerosol and cloud cover in reducing optical communication through the atmosphere in selected sites by ESA. In this work, a novel algorithm that uses both the Pearson correlation coefficient and Fourier analysis is used to assess such influences. Aerosol and cloud cover data are obtained from ground stations and satellite over Calern (France), Catania (Italy), Cebreros (Spain), and Lisbon (Portugal). The novel algorithm provides a preliminary long-, medium-, and short-term aerosol–cloud interaction for these four candidate sites, obtaining respectively the variability, the seasonal, and hourly trend of the aerosol concentration; the main medium-term periodicities of aerosols as clouds precursors; the short-term correlation between morning-afternoon aerosol concentration. The use of aerosols as a precursor parameter of cloud cover through a Fourier analysis, makes the algorithm versatile and usable for all sites of optical communication and astronomical importance in which optical transparency is a fundamental requirement, and therefore it is a potential tool to be developed to implement forecasting models.

Key words: Site Testing – detectors – Instrumentation – Algorithms – Optical Communication.

1 INTRODUCTION

The basic requirement for Optical Ground Station (OGS) sites is a good atmospheric transparency, and valid models of atmospheric turbulence analysis (Dali Ali et al. 2010; Giordano et al. 2014, 2021; Liu et al. 2015). The use of lasers to provide high-bandwidth optical connections is the basis of line-of-sight free-space optics (FSO) technology. The intensity of an FSO signal, in the case of optical paths of the order of kilometres, is reduced by the scattering and absorption of atmospheric particles. The signal can also shift and fluctuate due to spatial and temporal changes in atmospheric particulate absorption and concentration. The IR spectrum is characterized by various bands with high transmission through the free atmosphere and regions of low radiation transmission (near IR band from 1.5–1.7 μm). Atmospheric transmittance is determined with observational parameters for modelling to adjust the signal strength in an FSO communication link as a function of maximum reception. There are numerous existing and under-designed instruments for studying these parameters, atmospheric turbulence, and cloud cover (Cavazzani et al. 2014; Aristidi et al. 2019, 2020a, 2022). Usually, site testing is carried out with ground and satellite data and specifically at new sites, ground analysis campaigns require high costs and have a limited time coverage.

Satellite analyses overcome such limited time coverage, but they may contain bias due to the observational characteristics of the satellite used or to the particular site topography (Cavazzani et al. 2011; Cavazzani, Ortolani & Zitelli 2012, 2015; Cavazzani & Zitelli 2013). The main objective of this paper is to present a novel algorithm to estimate parameters (i.e. aerosols and cloud cover) affecting the atmospheric transparency within the framework of the ANAtOLIA (Atmospheric monitoring to Assess the availability of Optical Links through the Atmosphere) project funded by the European Space Agency (ESA). This international project aims at assessing the atmospheric conditions for optical communication at four ESA selected sites (see Fig. 1 and Table 1) named over Calern (France), Catania

★ E-mail: chiara.bertolin@ntnu.no

© 2023 The Author(s)
2023. Published by Oxford University Press on behalf of Royal Astronomical Society. This is an Open Access article distributed under the terms of the Creative Commons Attribution License (http://creativecommons.org/licenses/by/4.0/), which permits unrestricted reuse, distribution, and reproduction in any medium, provided the original work is properly cited.

Downloaded from https://academic.oup.com/rasti/article/2/1/420/7226210 by CNRS - ISTO user on 04 September 2023

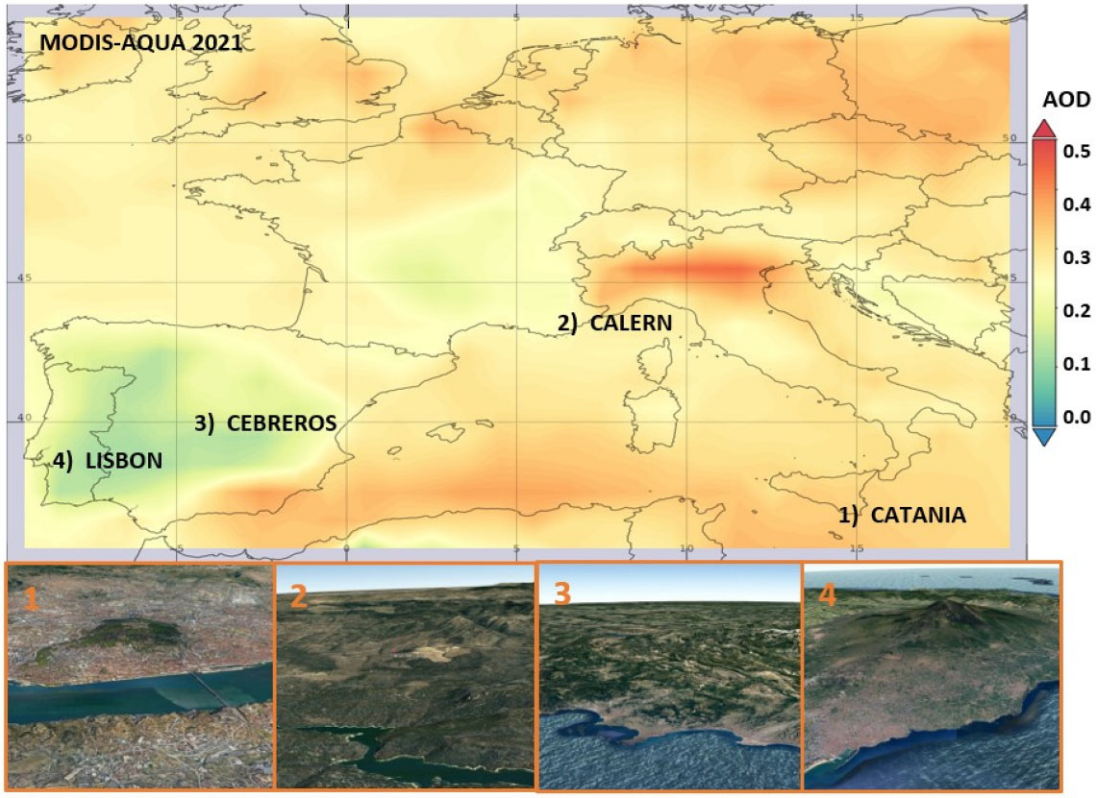

Figure 1. Location of the four sites involved in the analysis on the annual AOD time average map measured by *Aqua* satellite in 2021. As seen in the inserts the selected sites presents very different topographic conditions.

(Italy), Cebreros (Spain), and Lisbon (Portugal) (Ziad et al. 2022). The algorithm described overcomes satellite detection limitations by cross-correlating data from two polar satellites with ground data. Although this study is a preliminary analysis, however the heterogeneity of the ANAtOLIA sites already allows us to verify the close correlation between aerosols and cloud cover under different topographic conditions. Then the empirical calibration of satellite with ground-based data makes the aerosol–cloud interaction model exportable, for all sites of optical communications and astronomical importance where it is possible to implement weather forecasting models.

Specifically, the work has a double aim: the study of the long, medium, and short-term trends of the aerosols (aerosol optical depth, AOD), and their role as cloud condensation nuclei (CCN) (Anwar et al. 2022; Almeida et al. 2023). The study of aerosol–cloud interactions has important and multidisciplinary scientific implications, also in relation to the Earth's climate and its changes, as demonstrated by the numerous publications (Ackerman, Toon & Hobbs 1994; Deshler 2003; Seiki et al. 2014; Svensmark et al. 2017; Liu et al. 2020; Kiran et al. 2022). This contribution is therefore useful to understand such interactions.

The paper outline is as follows: Section 2 Data and algorithm, Section 3 Sites and results, Section 4 Discussion and conclusion.

2 SATELLITE AND GROUND BASED DATA

In the last decades, the site testing was greatly improved with the use of the satellite data to integrate traditional meteorological information retrieved at ground-based weather stations. The Moderate Resolution Imaging Spectroradiometer (MODIS) instrument mounted on the *Terra* and *Aqua* satellite observes the entire surface of the Earth twice a day (*Terra* in the morning and *Aqua* in the afternoon), with its 36 spectral bands ranging from 0.405 to 14.385 μm that acquire data at three spatial resolutions: 0.250, 0.500, and 1.000 km. *Terra* is the first EOS (Earth Observing System) platform and provides global data on the state of the atmosphere, land, and oceans, as well as their interactions with solar radiation. It has a near polar sun-synchronous orbit that passes over the equator at 10:30 a.m. (south to north) and 10:30 p.m. (north to south) in local solar time (Altitude 705 km, inclination 98.1 deg, and period 98.88 min). *Aqua* is a near polar sun-synchronous orbit satellite (Altitude 705 km, inclination 98.2 deg, and period 98.8 min). It passes over the equator at 1:30 p.m. (south to north) and 1:30 a.m. (north to south). Besides *Terra* and *Aqua*, this work also uses data from the polar Aura satellite: it has an orbit with an inclination of 98.22 deg and a period of 98.83 min, with a perigee of 708 km and an apogee of 710 km.

The Ozone Monitoring Instrument (OMI) tool, with which Aura is equipped, uses imaging to observe back scattered solar radiation in the visible and ultraviolet. Earth is seen in 740 wavelength bands along the satellite track, with an area large enough to provide global coverage. The maximum spatial resolution is 13 × 13 km to detect and track sources of pollution on an urban scale. In this analysis, the entire satellite archive of aerosol optical depth (AOD) and cloud fraction (CF) is used. The AOD defines how aerosols hinder the light transmission by absorption or dispersion. Mathematically, the AOD is defined as the integrated extinction coefficient on a vertical column of unit cross-section. The extinction coefficient is the fractional depletion of radiance per unit of path length, also called attenuation. The multiple wavelength AOD analysis provides Angstrom Exponent (AE). AE is used to study the size of aerosols and to derive the AOD

Downloaded from https://academic.oup.com/rasti/article/2/1/420/7226210 by CNRS - ISTO user on 04 September 2023

Figure 2. High spatial resolution (small rectangle 10 km × 10 km) versus low spatial resolution (wide rectangle 100 km × 100 km) coverage comparison at Calern. Figure shows that the use of the high spatial resolution is not sufficient in the case of a partially covered sky.

as a function of the wavelength (Loeb et al. 2008). The dependence on the atmospheric dust dimensions of the cloud–aerosol interaction and the AE in-depth analysis in relation to the optical communication will be dealt with in future works, being at the moment not significant for the primary aims of this contribution.

The CF is obtained by dividing the number of cloudy pixels by the total number of pixels. It also refers to the fraction of the sky covered by the various types of clouds (cirrus clouds, contrails, cumulus clouds, etc.), the physical state of their particles (solid, liquid, gaseous, or mixed), height of the clouds (low, medium, high), or all cloud types (total cloud fraction). The clouds differ from the fog, close to the surface, only in the altitude. In this work, the ground data for hourly analysis and validation of satellite data are provided by the Aerosol RObotic NETwork (AERONET)[1] that is a ground-based remote sensing network of aerosols. The AERONET project provides a long-term public domain database of the optical, physical, and radiative properties of aerosols for their research and characterization with global observations of the AOD. Version 3 AOD data are calculated for three levels of data quality: Level 1.0 (unscreened), Level 1.5 (cloud-screened and quality controlled), and Level 2.0 (quality assured).

2.1 Satellite data acquisition

The satellite data of this work is processed with Geospatial Interactive Online Visualization ANd aNalysis Infrastructure (GIOVANNI)[2] that is a Web-based application developed by the Goddard Earth Sciences Data and Information Services Center (GES DISC) with a simple and intuitive way to visualize, analyse, and access vast amounts of Earth science remote sensing data. In this analysis, per each site, a 1.0° × 1.0° matrix (*Terra* and *Aqua* satellite) is used. The matrix mean value drastically reduces the noise of the images. Fig. 2 shows that a higher spatial resolution (in the small rectangle), 10 km × 10 km wide, does not cover a sufficiently wide sky area above the site because it corresponds to a small geometric field of view as seen from the ground. The 0.25° × 0.25° OMI data are used for a cross-validation of MODIS data with lower spatial resolution. Fig. 3 shows the comparison between the two time series at different spatial resolution and different wavelength, the noise reduction is evident while the Pearson correlation coefficient between the two time series is 0.90. Therefore, for the aim of this work, the signal with less noise and greater field of view is selected, the correlation guarantees the validity of the data analysis and the periodicity of the time series.

Fig. 4 shows the MODIS-Aqua time series at the Calern site with their respective 30-d moving averages and linear regressions. A percentile statistical analysis is performed on the satellite and ground AOD time series to extrapolate the annual, seasonal, and daily hourly trend of the aerosols (see Figs 5 and 6, respectively). This analysis allows us to identify a typical yearly pattern by predicting the months and times with the highest concentration of aerosols.

In addition, the medium-term aerosol–cloud interactions is provided by a novel Fourier analysis application. The mathematical foundations with the related error, and the various applications are provided in Cavazzani, Ortolani & Zitelli (2017), Cavazzani et al. (2019, 2020b), and Bertolin et al. (2022). The Fast Fourier Transform (FFT) is applied to the time series of AOD and CF at the four sites (see Fig. 7). The analysis extrapolates the main periodicities with the relative phases. By exploiting the cyclic nature of the two phenomena, a double interprediction of the AOD and CF peaks is obtained. It is worthy to mention that although optical communication is heavily influenced by cloud cover and less influenced by aerosols, however aerosols are precursors of cloud cover itself. AOD monitoring becomes therefore essential for enhancing the predictive capability of the next cloud cover occurrence event, which may reduce optical communication link. So, the novel described algorithm is aimed at the ANAtOLIA project, but given its versatility and user-friendly applicability, it can be applied to any astronomical site location for early warning detection of the next cloud cover occurrence starting from the monitoring of the AOD, being of support to the current weather forecasting models.

Finally, the proposed methodological approach applied to short-term forecast exploits a simple but effective correlation between the *Terra* and *Aqua* satellites. The high correlation value allows for a reliable short-term morning–afternoon and afternoon–morning forecast because, by monitoring the AOD (or CF) in the morning with *Terra*, it is possible to predict the *Aqua* measurement in the afternoon and vice versa.

3 SITES ANALYSIS AND RESULTS

In this Section, the results of the novel long-, medium-, and short-term aerosol–cloud interactions algorithm at the four candidate sites for the ANAtOLIA project are reported. Cross-validated satellites and ground data provide a complete prediction for atmospheric optical transmissions. Furthermore, the versatility of the described methodologies allows the export of the aerosol–cloud interactions model for purely astronomical applications and for further implementation of weather forecast models. All data are freely accessible and cover the entire globe, except for the AERONET data that is a network with ground-based localized sites. The long- and medium-term study provides insight into the relationship between AOD and CF. Fourier's mathematical analysis of periodicities indicates the role of aerosols as concentration nuclei for clouds and precursor factor of cloud cover.

Aerosols obstruct optical communication in the atmosphere at wavelengths of 1064 and 1550 nm only when they are present in high concentrations, while cloud cover remains the major limitation. Under the previous hypotheses, however, the analysis of atmospheric particulate plays a key role in the success of the ANAtOLIA project, with a double result in the case of clear sky. The first result is the direct analysis of the typical aerosol occurrence and the classification of the months and times at greatest risk of high aerosol concentrations, while the second is the early forecast of cloud cover thanks to the growing time required to observe CF after the AOD peak

[1] https://aeronet.gsfc.nasa.gov/
[2] https://giovanni.gsfc.nasa.gov/giovanni/

Downloaded from https://academic.oup.com/rasti/article/2/1/420/7226210 by CNRS - ISTO user on 04 September 2023

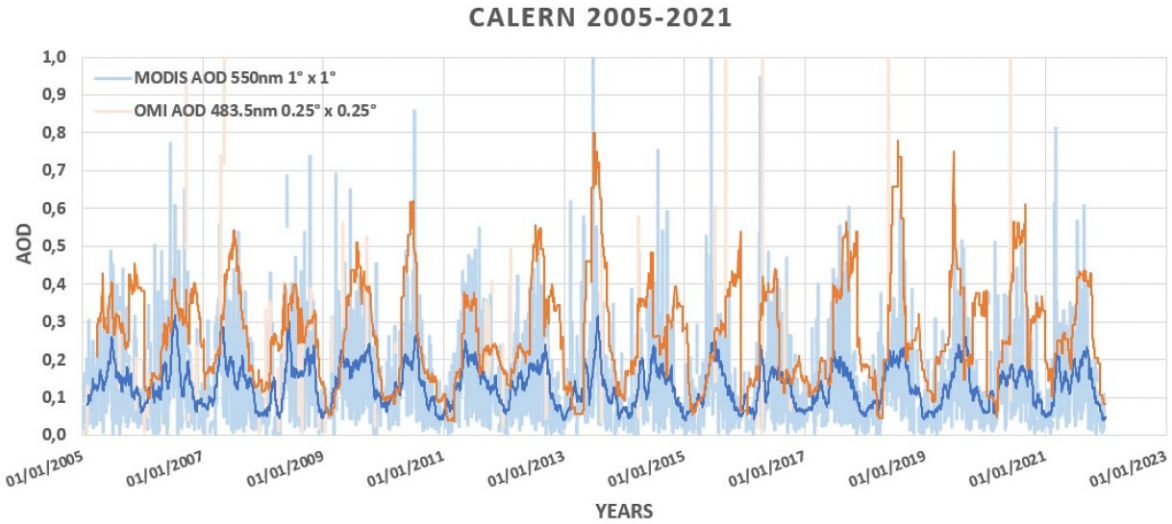

Figure 3. Comparison of AOD retrieved by MODIS and OMI on board of the two satellites with different spatial resolutions (2005–2021). The translucent lines describe the daily values, while the solid lines the 30-d moving average. The Pearson correlation coefficient between the two time series is 0.90.

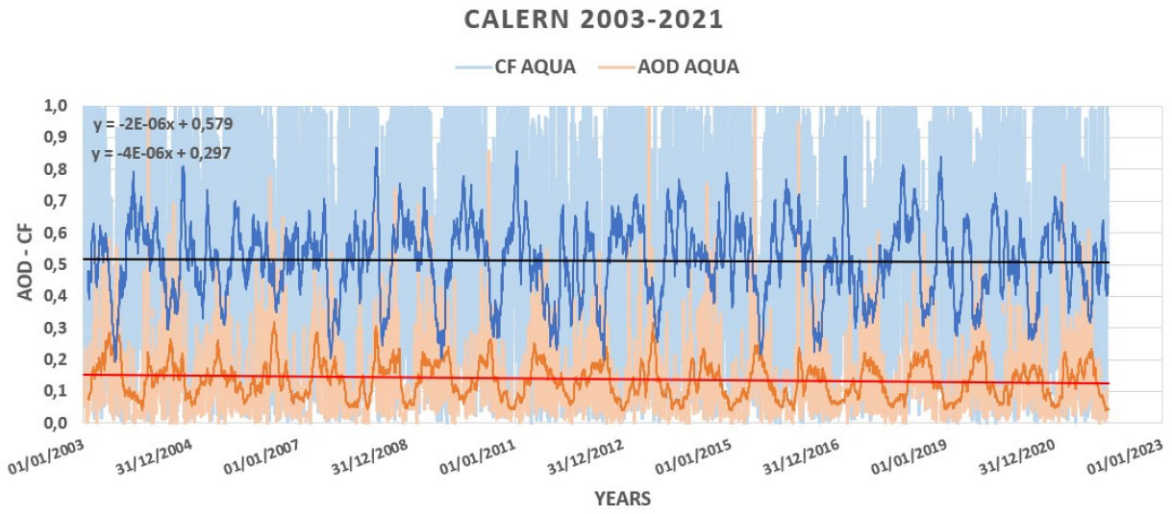

Figure 4. Trends of the daily time series of CF and AOD (Aqua, 2003–2021), with their respective 30-d moving averages and linear regressions, measured by MODIS-Aqua at the Calern site. The y-axis simultaneously indicates the cloud cover fraction (CF) and the aerosol optical depth (AOD). The equations of the regression lines and its angular coefficient (M) in the upper left provide an estimate of the long-term trend of cloud cover ($M_{\mathrm{CF}} = -2.0 \times 10^{-6}\,\mathrm{d}^{-1}$) and aerosols ($M_{\mathrm{AOD}} = -4.0 \times 10^{-6}\,\mathrm{d}^{-1}$).

occurrence. In the following subsections, the results for each site are presented, showing the cloud cover and ground gain statistics over the last 30 yr.

3.1 Calern, France

The Observatory of the Cote d'Azur Calern is located at an altitude of 1260 a.s.l, and it is the reference site of the ANAtOLIA project and the site at highest altitude among those analysed. It is located about 25 km far from the sea. Table 2 shows the statistics of the ground weather stations[3] over the last 30 yr (1991–2020) at the Calern site. The first column shows the month, the second, third, fourth, and fifth columns, respectively, show daily mean fraction of clear days (ClDF), fraction of mixed days (MDF), fraction of cloudy days (CDF), and fraction of days with precipitation (RDF). The sixth column gives the monthly total precipitation (P), as the optical communication is in fact ineffective in case of precipitation (Zeller et al. 2010).

Table 3 describes the results of our novel long- (columns 1, 2, and 3), medium- (columns 4 and 5), and short-term (column 6) aerosol–cloud interaction algorithm at the Calern site. The first column above gives the slopes with the associated uncertainties of the linear regressions ($y = Mx + Q$, y is the AOD or CF value and x is the observation date) calculated on the AOD and CF time series measured with MODIS, and shown in Fig. 4.

[3] https://www.meteoblue.com/

Downloaded from https://academic.oup.com/rasti/article/2/1/420/7226210 by CNRS - ISTO user on 04 September 2023

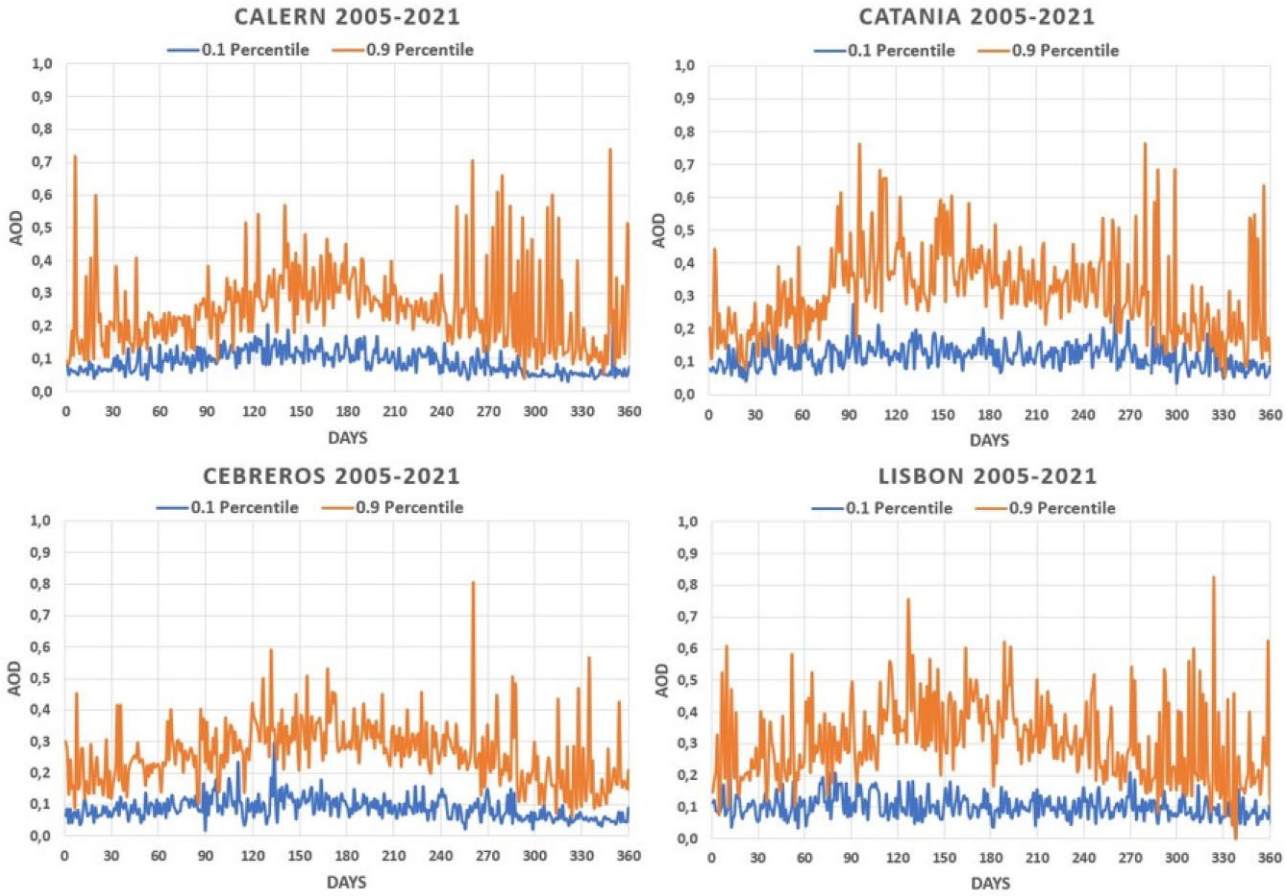

Figure 5. Percentile analysis of AOD OMI data (2005–2021) from *Aura* satellite at the four sites. Site panels show annual and seasonal aerosol trends and some anomalous months at seasonal changes.

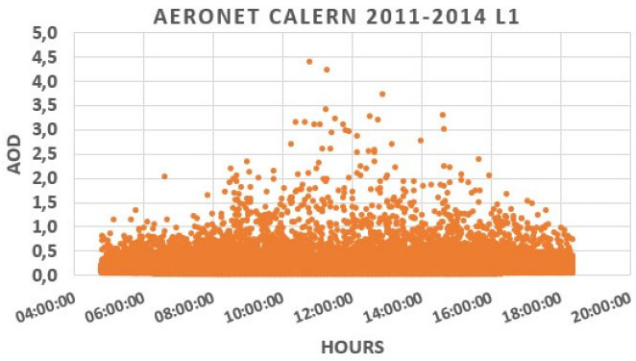

Figure 6. Hourly percentile analysis from AERONET data at the Calern site (2011–2014). The dots show the daily trend of concentrated aerosols between 10:00 and 15:00 (local solar time).

The uncertainties for the angular coefficient (M) and the linear regression intercept (Q) are provided by the following equations (Taylor 1999):

$$\sigma_M = \sigma_y \sqrt{\frac{N}{\Delta}}, \tag{1}$$

$$\sigma_Q = \sigma_y \sqrt{\frac{\sum x_i^2}{\Delta}}, \tag{2}$$

where N is the number of values, σ_y, and Δ are given by the equations:

$$\sigma_y = \sqrt{\frac{1}{N-2}\sum (y_i - Mx_i - Q)^2}, \tag{3}$$

$$\Delta = N\sum x_i^2 - \left(\sum x_i\right)^2. \tag{4}$$

The statistical sample ($N = 6940$ d) provides the uncertainties $\sigma_{M,\mathrm{AOD}} = 2.0 \times 10^{-8}\,\mathrm{d}^{-1}$, $\sigma_{Q,\mathrm{AOD}} = 5.8 \times 10^{-3}$ and $\sigma_{M,\mathrm{CF}} = 1.3 \times 10^{-8}\,\mathrm{d}^{-1}$, $\sigma_{Q,\mathrm{CF}} = 3.8 \times 10^{-3}$, respectively. These values corresponding to a percentage error <1.0 percent validate the slopes of the linear regressions used to estimate long-term trends. The data provides a first indicative estimate of the relationship between the two parameters (AOD and CF).

The decrease of both values provides a first confirmation of the hypothesis of this contribution that is considering aerosols as precursors of cloud. In fact, when aerosols decrease, the CF decreases as well. The AOD decreases by $-4.0 \times 10^{-6}\,\mathrm{d}^{-1}$, while the CF by $-2.0 \times 10^{-6}\,\mathrm{d}^{-1}$. At the bottom in the first column, the AOD and CF mean value measured from 2003 to 2021 is reported. The uncertainties ($\Delta\bar{y}$) on the mean values ($\bar{y}$) are obtained from the equation (Taylor 1999):

$$\Delta\bar{y} = \frac{1}{\sqrt{N}}\sqrt{\frac{\sum (y_i - \bar{y})^2}{(N-1)}}, \tag{5}$$

Downloaded from https://academic.oup.com/rasti/article/2/1/420/7226210 by CNRS - ISTO user on 04 September 2023

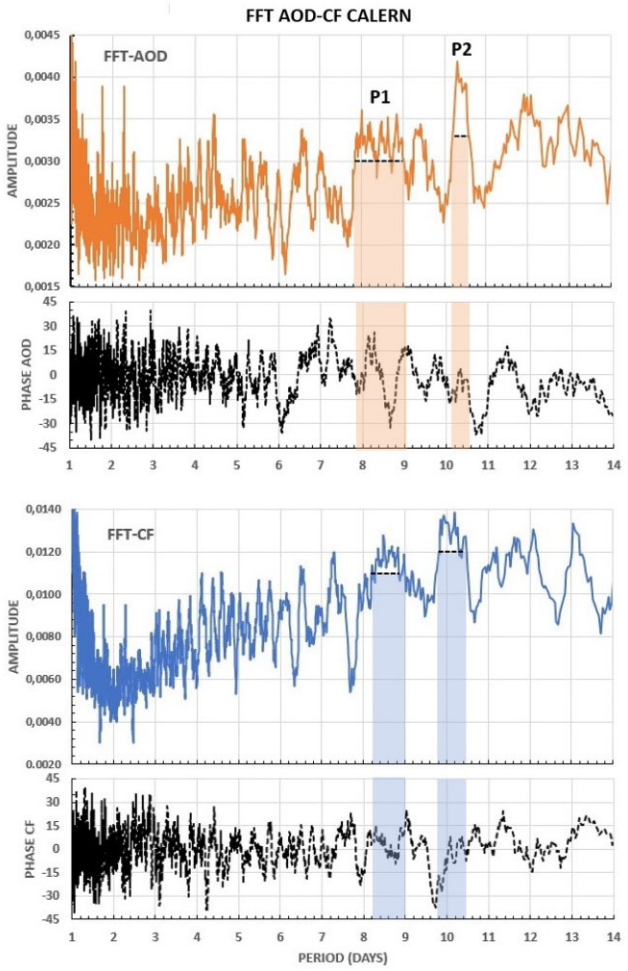

Figure 7. FFT of the MODIS-Aqua AOD and CF time series (2003–2021) at the Calern site (Top panel: amplitude; bottom panel: phase in degrees).

Table 1. Geographic characteristics of the analysed sites, and satellite instruments used.

Site	Latitude	Longitude	Altitude (m)
Calern	43.75	6.92	1260
Catania	37.49	15.07	200
Cebreros	40.45	−4.46	720
Lisbona	38.73	−9.15	100
	Spatial resolution	Spectral range (nm)	
MODIS	1.0° × 1.0°	405–14385	
OMI	0.25° × 0.25°	270–500	

where y is the measured AOD or CF value. The uncertainty analysis gives the values of 1.1×10^{-3} for AOD and 1.1×10^{-3} for CF, corresponding to percent errors respectively of 0.79 per cent and 0.22 per cent.

The top left-hand panel of the Fig. 5 shows the percentile analysis of the AOD time series at the Calern site. The 0.1 percentile and the 0.9 percentile depict the annual and seasonal range of aerosols and evaluate the months at risk of transmission: low risk (LR) AOD < 0.2, medium risk (MR) 0.2 < AOD < 0.4, high risk (HR) AOD > 0.4 (see column 2 of Table 3). The 0.1 percentile describes the trend of the year with lower AOD values while the 0.9 percentile describes the year with higher values, therefore the area between the two trends represents the range of AOD values as a function of the typical year.

Table 2. Statistical analysis of the mean ground-based weather conditions at the Calern site from 1991 to 2020. Clear days fraction (ClDF), mixed days fraction (MDF), cloudy days fraction (CDF), rainy days fraction (RDF), and precipitation (P).

Month	ClDF per cent	MDF per cent	CDF per cent	RDF per cent	Precipitation (mm)
Jan	36	33	31	28	71
Feb	33	40	27	26	42
Mar	29	44	27	28	52
Apr	16	52	32	39	68
May	20	56	24	34	52
Jun	29	62	9	29	31
Jul	42	53	5	22	22
Aug	38	56	6	19	15
Sep	29	56	15	24	38
Oct	27	46	27	27	79
Nov	32	34	34	32	99
Dec	38	31	31	28	25

In column 2 of Table 3 the average monthly risk for Calern is reported. Fig. 6 shows Level 1.0 AERONET hourly data from 2011 to 2014 at 500 nm at the Calern site. We extrapolated the times to aerosol LR, MR, and HR reported in column 3 of the Table 3. This categorization is also important to detect natural hazards that may trigger HR aerosol outbreaks. This result schedules months and times for communications or astronomical observations with less risk of atmospheric perturbations. Level 1.0 AERONET data are not shielded for thin clouds. We used this time series to assess the risks even in the presence of thin clouds not detected by satellites. The greater number of data compared to Level 1.5 and 2.0 provides a greater distribution, highlighting the trend of aerosols during the day.

The medium-term aerosol–cloud interactions provided in columns 4 and 5 of Table 3 is based on Fourier analysis of the time series of AOD and CF. Fig. 7 shows the FFT of AOD (FFT_{AOD}) with its phase (top panel) and the FFT of CF (FFT_{CF}) with its phase (bottom panel) at the Calern site. The FFT_{AOD} trend detects a first significant peak at 8.4 ± 0.6 d (P1), this peak due to the complexity of aerosol observation has a full width at half-maximum (FWHM) of 1.2 d, highlighted by the coloured area. The first significant peak is defined in correlation to the cloud FFT (e.g. Aerosol–cloud interaction uses period-correlated peaks recorded in the period between 7 and 15 d with an amplitude greater than 75 per cent of the maximum amplitude. The low signal-to-noise ratio of the FFT in the first 7 d prevents the detection of significant peaks in terms of time duration.) A second uncertainty, based on the frequency resolution of the Fourier analysis, is calculated with the perturbation periodicity P_P formula:

$$P_P = \frac{1}{f} \pm \frac{P_P^2}{2T}, \tag{6}$$

where P_P is the peak periodicity and T is the entire observation period over which the FFT is applied. This dispersion is not significant considering a peak of 8.4 d over an observation period of 20 yr, so we use the uncertainty found with the FWHM of 1.2 d (±0.6 d). The same procedure detects a peak cloud cover at 8.6 ± 0.4 d. The second periodicities (P2) detected are 10.4 ± 0.2 d for aerosols and 10.1 ± 0.3 for clouds. This confirms the common periods between the two phenomena in the dispersion margins.

Downloaded from https://academic.oup.com/rasti/article/2/1/420/7226210 by CNRS - ISTO user on 04 September 2023

Table 3. Long, medium, and short time aerosol–cloud interactions at Calern based on data from 2003 to 2021. The top box of column 1 shows the slope of the linear regression (Angular coefficient M) of the AOD and CF time series with the associated uncertainties. The AOD and CF mean value and its uncertainty are reported in the lower box of column 1. Column 2 gives the low risk (LR), medium risk (MR), and high risk (HR) months for aerosol content and column 3 the risk during the day times. The medium-term aerosol–cloud interactions is described in columns 4 and 5. The main periodicities of AOD and CF are shown with the relative error calculated with FWHM and the relative phases. Column 6 reports the Pearson correlation coefficient between Aqua-Terra for AOD and CF for short-term forecast (Morning-Afternoon Correlation Coefficient, MACC).

	Long-term		Medium-term		Short-term
Angular coefficient MODIS (d^{-1})	Monthly OMI	Hourly AERONET	AOD FFT MODIS	CF FFT MODIS	MACC Aqua-Terra
$M_{AOD} = -4.0 \times 10^{-6}$	Jan. HR	08–10 a.m. LR	Periodicity 1	Periodicity 1	$MACC_{AOD} = 0.89$
$\sigma_{M,\,AOD} = \pm 2.0 \times 10^{-8}$	Feb. MR	10–12 a.m. MR	8.4 ± 0.6 d	8.6 ± 0.4 d	$MACC_{CF} = 0.88$
$M_{CF} = -2.0 \times 10^{-6}$	Mar. LR	12–14 p.m. HR	Periodicity 2	Periodicity 2	–
$\sigma_{M,\,CF} = \pm 1.3 \times 10^{-8}$	Apr. LR	14–16 p.m. MR	10.4 ± 0.2 d	10.1 ± 0.3 d	–
	May MR	16–18 p.m. LR	Phase 1	Phase 1	–
Mean value	Jun. MR	–	$+5° \Rightarrow -2h - 50$ arcmin	$-10° \Rightarrow +7h10$ arcmin	–
MODIS	Jul. MR	–	Phase 2	Phase 2	–
AOD = 0.14	Aug. LR	–	$+5° \Rightarrow -3h50$ arcmin	$-5° \Rightarrow +3h20$ arcmin	–
ΔAOD $= 1.1 \times 10^{-3}$	Sep. HR	–	–	–	–
CF = 0.51	Oct. HR	–	–	–	–
$\Delta CF = 1.1 \times 10^{-3}$	Nov. HR	–	–	–	–
	Dec. HR	–	–	–	–

The aerosol–cloud interactions can be derived from the phases of the signals (see columns 4 and 5 of Table 3). Fig. 8 zooms in on the 8.4-d amplitude peak of AOD (top panel) with its phase (bottom panel). The solid line represents the 15-d moving average of the two signals. The dashed line in the top panel is the FWHM (1.2 d). The +5 deg phase of this peak, corresponding to 2 h and 50 min, is obtained by averaging the phase values for this dispersion (dashed line – bottom panel). The first aerosol peak (P1) is about 10 h ahead of the cloud cover peak, while the second aerosol peak (P2) is about 7 h ahead of the cloud cover peak, adding the phase shifts. The complexity of the two signals analysed provides an estimate of this phase difference within a margin of error of 0.5 d, corresponding to 12 h. The significant result is the mathematical demonstration that aerosols are precursors of clouds and can be used as a forecasting parameter. Further investigations will be carried out during the project. The ground data reported in the Table 2 can be correlated to the Fourier analysis: the fractions of overcast sky lead to the hypothesis that during January, February, March, April, October, November, and December the perturbations are not distinct (e.g. we have on average 3/4 covered days three times a month).

Finally, the short-term forecast is based on the correlation between the *Terra* and *Aqua* satellites, the first passes during the morning while the second during the afternoon. Fig. 9 shows the map of the entire area containing the four sites under examination. The top panel calculates the correlation for AOD, while the bottom panel calculates the correlation for CF. Pearson correlation coefficient values greater than 0.8 over the entire area make this morning-afternoon and afternoon-morning forecast very useful for short-term scheduling of optical communications in the atmosphere. Fig. 10 displays this correlation for AOD (left-hand panel) and CF (right-hand panel). The Pearson correlation coefficient is 0.89 for AOD and 0.88 for CF at the Calern site.

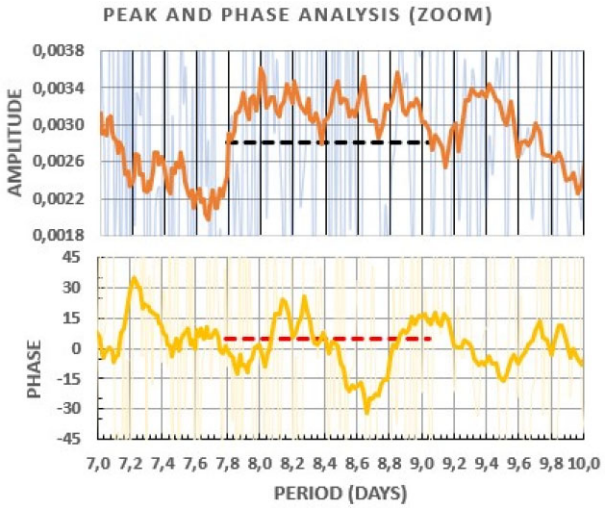

Figure 8. Analysis of the peak periodicity (P1-Fig.7 Zoom) for the amplitude (top panel) and the phase (bottom panel). FWHM represents signal dispersion (dashed line – top panel). Phase is derived from the average phase bounded by the dotted line in the bottom panel.

3.2 Catania, Italy

The second site analysed is the Astrophysical Observatory of Catania, INAF research facility and the Astrophysics section of the Department of Physics and Astronomy of the University of Catania. The privileged geographical position of Catania, a predominantly clear sky site in southern Italy below Etna (3340 m a.s.l.), the largest active volcano in Europe (Corsaro et al. 2017; Magee, Ubidea & Caulfieldab 2021; Sahoo et al. 2022), has made possible almost 100 yr of uninterrupted observation of solar activity. These characteristics are of interest for the ANAtOLIA project, which can make use of the existing infrastructure.

Table 4 shows the statistics of the ground weather stations over the last 30 yr (1991–2020) at the Catania site. The mean percentage of fully covered days is 18 per cent. This guarantees the site a great continuity of observation. The top right-hand panel of Fig. 5 shows the AOD percentile analysis at the Catania site. The case study of a similar site, subject to occasional volcanic eruptions, provides the

Downloaded from https://academic.oup.com/rasti/article/2/1/420/7226210 by CNRS - ISTO user on 04 September 2023

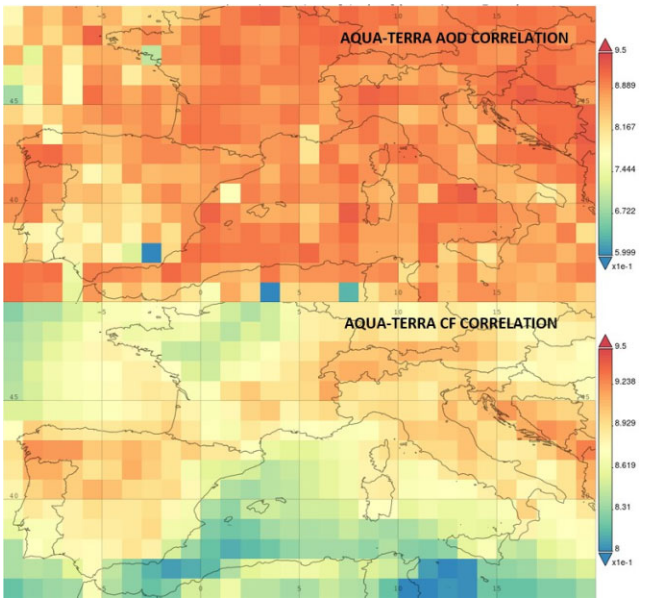

Figure 9. Correlation map between MODIS *Terra* and *Aqua* of AOD (top panel) and CF (bottom panel).

possibility of analysing unique conditions with reference to outbreak of atmospheric particulate matter. Table 5 describes the results of the optical transmission aerosol–cloud interaction algorithm at the Catania site. The AOD decreases by $-4.0 \times 10^{-6}\,\mathrm{d}^{-1}$, and the CF by $-2.0 \times 10^{-6}\,\mathrm{d}^{-1}$, also in this case. This could be a common feature of Mediterranean basin sites. The Catania site is more frequently contaminated by aerosols, with a periodic peak every 6.5 ± 0.3 d and every 10.8 ± 0.4 d. Volcanic activity is an important factor to consider and investigate. The duration of the ANAtOLIA project will allow deepening this aspect in future works. The dispersion margins

Table 4. Statistical analysis of the mean ground-based weather conditions at the Catania site from 1991 to 2020. Clear days fraction (ClDF), mixed days fraction (MDF), cloudy days fraction (CDF), rainy days fraction (RDF), and Precipitation (P).

Month	ClDF per cent	MDF per cent	CDF per cent	RDF per cent	Precipitation (mm)
Jan	19	43	38	37	67
Feb	19	51	30	36	53
Mar	22	52	26	29	44
Apr	18	61	21	29	37
May	27	63	10	18	15
Jun	45	51	4	13	9
Jul	59	41	0	11	6
Aug	58	41	1	14	8
Sep	34	58	8	28	32
Oct	25	57	18	28	34
Nov	19	54	27	30	49
Dec	21	45	34	33	70

correlate these peaks with the cloud cover periodicities at 6.8 ± 0.4 and 10.2 ± 0.5 d, respectively. The phenomena associated with the two periodicities may be closely related, the first phenomenon may be of small intensity (particularly in the spring and summer months), as confirmed by the data from the ground, and therefore be traced back to the second perturbation. Fig. 10 displays this correlation for AOD (left-hand panel) and CF (right-hand panel). The Pearson correlation coefficient is 0.84 for AOD and 0.87 for CF at the Catania site. The lower correlation could be due to volcanic eruptions.

3.3 Cebreros, Spain

The Cebreros site is near the CESAR Cebreros Optical Telescope, where the ESA's Deep Space Tracking Station is located. A sky quality observation campaign is underway at the Cabauw

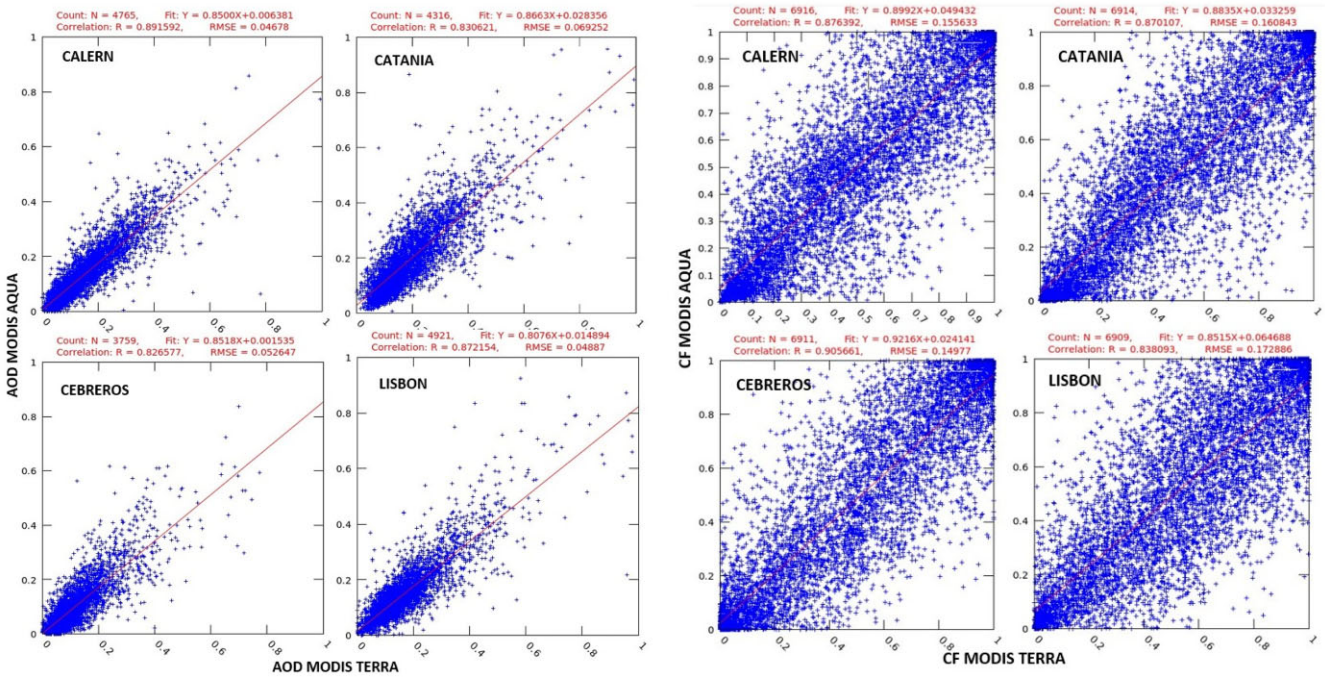

Figure 10. AOD (left-hand panel) and CF (right-hand panel) MODIS *Terra–Aqua* (2003–2021) correlation at the four candidate sites of the ANAtOLIA project.

Downloaded from https://academic.oup.com/rasti/article/2/1/420/7226210 by CNRS - ISTO user on 04 September 2023

Table 5. Long, medium, and short time aerosol–cloud interactions at Catania based on data from 2003 to 2021. The top box of column 1 shows the slope of the linear regression (Angular coefficient M) of the AOD and CF time series with the associated uncertainties. The AOD and CF mean value and its uncertainty are reported in the lower box of column 1. Column 2 gives the low risk (LR), medium risk (MR), and high risk (HR) months for aerosol content and column 3 the risk during the day times. The medium-term aerosol–cloud interactions is described in columns 4 and 5. The main periodicities of AOD and CF are shown with the relative error calculated with FWHM and the relative phases. Column 6 reports the Pearson correlation coefficient between *Aqua-Terra* for AOD and CF for short-term forecast (Morning-Afternoon Correlation Coefficient, MACC).

	Long-term		Medium-term		Short-term
Angular coefficient	Monthly	Hourly	AOD FFT	CF FFT	MACC
MODIS (d^{-1})	OMI	AERONET	MODIS	MODIS	Aqua-Terra
$M_{AOD} = -5.0 \times 10^{-6}$	Jan. LR	08–10 a.m. LR	Periodicity 1	Periodicity 1	$MACC_{AOD} = 0.83$
$\sigma_{M,\,AOD} = \pm 1.9 \times 10^{-8}$	Feb. MR	10–12 a.m. MR	6.5 ± 0.3 d	6.8 ± 0.4 days	$MACC_{CF} = 0.87$
$M_{CF} = -5.0 \times 10^{-6}$	Mar. LR	12–14 p.m. HR	Periodicity 2	Periodicity 2	–
$\sigma_{M,\,CF} = \pm 1.4 \times 10^{-8}$	Apr. HR	14–16 p.m. MR	10.8 ± 0.4 d	10.2 ± 0.5 days	–
	May MR	16–18 p.m. LR	Phase 1	Phase 1	–
Mean value	Jun. MR	–	$-10° \Rightarrow +4h20$ arcmin	$-20° \Rightarrow +9h20$ arcmin	–
MODIS	Jul. MR	–	Phase 2	Phase 2	–
AOD = 0.20	Aug. MR	–	$15° \Rightarrow -10h50$ arcmin	$10° \Rightarrow -6h40$ arcmin	–
$\Delta AOD = 1.5 \times 10^{-3}$	Sep. MR	–	–	–	–
CF = 0.48	Oct. HR	–	–	–	–
$\Delta CF = 1.2 \times 10^{-3}$	Nov. MR	–	–	–	–
	Dec. HR	–	–	–	–

Table 6. Statistical analysis of the mean ground-based weather conditions at the Cebreros site from 1991 to 2020. Clear days fraction (ClDF), mixed days fraction (MDF), cloudy days fraction (CDF), rainy days fraction (RDF), and Precipitation (P).

Month	ClDF per cent	MDF per cent	CDF per cent	RDF per cent	Precipitation (mm)
Jan	26	38	36	33	51
Feb	36	33	31	31	38
Mar	36	39	25	25	38
Apr	28	48	24	35	46
May	28	53	19	33	40
Jun	49	44	7	18	17
Jul	72	26	2	9	6
Aug	61	36	3	10	6
Sep	45	44	11	18	23
Oct	32	41	27	27	56
Nov	30	36	34	31	63
Dec	30	31	39	35	64

Experimental Site for Atmospheric Research (CESAR) telescope site aimed at best estimates of flux sensitivity and photometric stability in relation to meteorological and observational statistics, local meteorology, atmospheric optical extinction, seeing, optical turbulence profiles, water vapour content, and wind vector (Ventura et al. 2009; Fernandez et al. 2015; Ammerlaan et al. 2017; Bosveld et al. 2020). The synergy with other projects provides therefore an added value for the ANAtOLIA project.

Table 6 shows the statistics of the ground weather stations over the last 30 yr (1991–2020) at the Cebreros site. Table 7 describes the results of our aerosol–cloud interaction algorithm at the Cebreros site. The Cebreros site has the lowest AOD, the distance from the sea does not make it subject to marine aerosol presence. The AOD decreases by $-9.0 \times 10^{-7}\,d^{-1}$, and the CF by $-4.0 \times 10^{-6}\,d^{-1}$. The FFT detects two AOD peaks at 7.5 ± 0.2 and 10.8 ± 0.4 corresponding to two CF peaks at 7.5 ± 0.4 and 10.4 ± 0.5 respectively in the 15-d interval. The two signals have the same periodicity in the dispersion limits, with an AOD phase advance of about 12 h for the first peak, and about 4 h for the second peak.

On average, there are three meteorological perturbations per month of variable duration with the seasonal period. The mean winter (Dec., Jan., Feb.) CDF is 35 percent, spring (Mar., Apr., May.) and fall (Sep., Oct., Nov.) CDF is 23–24 percent, and summer (Jun., Jul., Aug.) CDF is 4 percent, corresponding to average atmospheric perturbations of about 4–3, 3–2, and 1.5 d, respectively.

3.4 Lisbon, Portugal

The Lisbon Astronomical Observatory is internationally recognized for its quality work in the field of astronomy. It has been managed by the University of Lisbon since 1992, responsible for scientific and historical research, and for media relations.

Table 8 shows the statistics of the ground weather stations over the last 30 yr (1991–2020) at the Lisbon site. The results of the short-, medium-, and long-term aerosol–cloud interaction algorithm are described in Table 9. This is the only site of those studied, where the linear regressions of AOD and CF are inversely proportional. The AOD decreases by $-2.0 \times 10^{-6}\,d^{-1}$, while the CF increases by $+2.0 \times 10^{-6}\,d^{-1}$. This could depend on a MODIS bias when detecting mixed scenes over the Atlantic Ocean (Cavazzani et al. 2015), or on the high presence of marine aerosol detected as a cloud rather than as an atmospheric particulate. The duration of the project will guarantee to deepen this point.

The bottom right-hand panel of Fig. 5 shows the AOD percentile analysis at the Lisbon site. The high AOD of the winter months may depend on marine aerosols in the event of winter Atlantic perturbations. On this site, the relationship between AOD and CF obtained from the FFT is evident, they recall two AOD main periodicities at 8.6 ± 0.2 and 12.4 ± 0.6 d corresponding to two CF periodicities at 8.4 ± 0.4 and 12.2 ± 0.6 d. The AOD phase advance appears to be a bit more than 5 and 12 h, respectively. The short-term correlations referring to the Fig. 10 are 0.88 for AOD and 0.84 for CF.

Downloaded from https://academic.oup.com/rasti/article/2/1/420/7226210 by CNRS - ISTO user on 04 September 2023

Table 7. Long, medium, and short time aerosol–cloud interactions at Cebreros based on data from 2003 to 2021. The top box of column 1 shows the slope of the linear regression (Angular coefficient M) of the AOD and CF time series with the associated uncertainties. The AOD and CF mean value and its uncertainty are reported in the lower box of column 1. Column 2 gives the low risk (LR), medium risk (MR), and high risk (HR) months for aerosol content and column 3 the risk during the day times. The medium-term aerosol–cloud interactions is described in columns 4 and 5. The main periodicities of AOD and CF are shown with the relative error calculated with FWHM and the relative phases. Column 6 reports the Pearson correlation coefficient between *Aqua-Terra* for AOD and CF for short-term forecast (Morning-Afternoon Correlation Coefficient, MACC).

	Long-term		Medium-term		Short-term
Angular coefficient	Monthly	Hourly	AOD FFT	CF FFT	MACC
MODIS (d^{-1})	OMI	AERONET	MODIS	MODIS	*Aqua-Terra*
$M_{AOD} = -9.0 \times 10^{-7}$	Jan. MR	08–10 a.m. LR	Periodicity 1	Periodicity 1	$MACC_{AOD} = 0.83$
$\sigma_{M,\,AOD} = \pm 2.2 \times 10^{-8}$	Feb. LR	10–12 a.m. MR	7.5 ± 0.2 d	7.5 ± 0.4 d	$MACC_{CF} = 0.91$
$M_{CF} = -4.0 \times 10^{-6}$	Mar. MR	12–14 p.m. HR	Periodicity 2	Periodicity 2	–
$\sigma_{M,\,CF} = \pm 1.5 \times 10^{-8}$	Apr. MR	14–16 p.m. MR	10.8 ± 0.4	10.4 ± 0.5	–
	May HR	16–18 p.m. LR	Phase 1	Phase 1	–
Mean value	Jun. MR	–	$5° \Rightarrow -2h30$ arcmin	$-20° \Rightarrow +10h$	–
MODIS	Jul. MR	–	Phase 2	Phase 2	–
AOD = 0.10	Aug. MR	–	$10° \Rightarrow -7h10$ arcmin	$5° \Rightarrow -3h30$ arcmin	–
$\Delta AOD = 9.0 \times 10^{-4}$	Sep. MR	–	–	–	–
CF = 0.50	Oct. MR	–	–	–	–
$\Delta CF = 1.3 \times 10^{-3}$	Nov. HR	–	–	–	–
	Dec. MR	–	–	–	–

Table 8. Statistical analysis of the mean ground-based weather conditions at the Lisbon site from 1991 to 2020. Clear days fraction (ClDF), mixed days fraction (MDF), cloudy days fraction (CDF), rainy days fraction (RDF), and Precipitation (P).

Month	ClDF per cent	MDF per cent	CDF per cent	RDF per cent	Precipitation (mm)
Jan	29	37	34	29	51
Feb	28	45	27	29	45
Mar	32	44	24	24	40
Apr	28	53	19	25	37
May	31	55	14	21	27
Jun	45	50	5	7	6
Jul	57	41	2	4	2
Aug	49	48	3	5	2
Sep	42	49	9	14	18
Oct	34	46	20	28	57
Nov	30	43	27	29	65
Dec	26	40	34	32	71

4 DISCUSSION AND CONCLUSION

In this paper, we described a novel long-, medium-, and short-term aerosol–cloud interaction algorithm. The algorithm uses satellite (MODIS and OMI instruments) and ground-based (AERONET network) time series, and it is applied to the four sites selected by ESA within the ANAtOLIA project (see Fig. 1 and Table 1). This project aims at the selection, analysis and forecasting of atmospheric conditions at these ground-based sites for optical linkages through the atmosphere. The algorithm provides a long-, medium-, and short-term estimate of the aerosol–cloud interaction in relation to the useful observation time for astronomical sites or OGS, i.e. clear sky not affected by both AOD outbreaks and cloud fraction. The use of two satellite instruments (MODIS and OMI) with the relative correlation of 90 per cent (Fig. 3), compared with ground data of the last 30 yr (Tables 2, 4, 6, and 8), cross validates the results. The 90 per cent correlation between MODIS and OMI justifies the decrease in spatial resolution, the $1.0° \times 1.0°$ matrix reduces signal noise by increasing the signal-to-noise ratio (SNR). Fig. 2 also schematizes that a larger matrix increases the observational effectiveness in relation to astronomical observations at low zenithal angles or optical communication. The low-altitude rectangle represents the limit altitude with the highest concentration of aerosols (about 1000 m). The high-altitude rectangle represents the satellite field of view in relation to the spectral range of the weighting functions (Cavazzani et al. 2015). Under these hypotheses, MODIS has been used for both the long-term time analysis of AOD and CF as shown in the Fig. 4 and for the subsequent Fourier analysis for the medium-term aerosol–cloud interaction (Fig. 7). The long-term satellite archive (6940 d) gives an uncertainty of less than 1 per cent on the mean values and on the slopes of the linear regressions, validating their use for the long-term aerosol–cloud interaction estimation.

The FFT performs best with a high SNR. The percentile analysis in Fig. 5 uses OMI data, in this case, a greater spatial resolution reduces any bias due to the topography of the sites and the analysis may be more homogeneously compared with AERONET data from the ground (Fig. 6). A result of this work is the mathematical demonstration through the Fourier analysis reported in Fig. 7 of how aerosols are precursor of clouds, acting as CCN. Common periodicities between the discrete signal of AOD and CF in the medium-term (15 d), and within the limits of the FWHM peak, have been observed. The phase advance between the two signals demonstrates that aerosols are precursors of clouds, thus assuming a possible important predictive role that can be used in the future to implement forecasting models in relation to optical communication and astronomical observations. The peak phase is derived from the mean phase over the range limited by its FWHM (Fig. 8).

Finally, the AOD and CF short-term forecast is given by a simple and effective morning-afternoon correlation between the *Terra* and *Aqua* satellites. The Pearson correlation coefficient for the AOD is between 0.75 and 0.95, while for the CF it is between 0.80 and 0.95 for the entire area of the nations to which the sites in question belong (Fig. 9). The Pearson *Terra-Aqua* correlation for AOD and CF at the four candidate sites is described in Fig. 10 (4 left-hand panels and 4 right-hand panels, respectively).

Downloaded from https://academic.oup.com/rasti/article/2/1/420/7226210 by CNRS - ISTO user on 04 September 2023

Table 9. Long, medium, and short time aerosol-cloud interactions at Lisbon based on data from 2003 to 2021. The top box of column 1 shows the slope of the linear regression (Angular coefficient M) of the AOD and CF time series with the associated uncertainties. The AOD and CF mean value and its uncertainty are reported in the lower box of column 1. Column 2 gives the low risk (LR), medium risk (MR), and high risk (HR) months for aerosol content and column 3 the risk during the day times. The medium-term aerosol–cloud interactions is described in columns 4 and 5. The main periodicities of AOD and CF are shown with the relative error calculated with FWHM and the relative phases. Column 6 reports the Pearson correlation coefficient between *Aqua-Terra* for AOD and CF for short-term forecast (Morning-Afternoon Correlation Coefficient, MACC).

	Long-term		Medium-term		Short-term
Angular coefficient	Monthly	Hourly	AOD FFT	CF FFT	MACC
MODIS (d^{-1})	OMI	AERONET	MODIS	MODIS	Aqua-Terra
$M_{AOD} = -2.0 \times 10^{-6}$	Jan. HR	08–10 a.m. LR	Periodicity 1	Periodicity 1	$MACC_{AOD} = 0.87$
$\sigma_{M,\,AOD} = \pm 2.0 \times 10^{-8}$	Feb. MR	10–12 a.m. MR	8.6 ± 0.4 d	8.4 ± 0.4 d	$MACC_{CF} = 0.83$
$M_{CF} = +2.0 \times 10^{-6}$	Mar. MR	12–14 p.m. HR	Periodicity 2	Periodicity 2	–
$\sigma_{M,\,CF} = \pm 1.2 \times 10^{-8}$	Apr. MR	14–16 p.m. MR	12.4 ± 0.6 d	12.2 ± 0.6 d	–
	May HR	16–18 p.m. LR	Phase 1	Phase 1	–
Mean value	Jun. HR	–	$+10° \Rightarrow -5h50$ arcmin	$-20° \Rightarrow +11h10$ arcmin	–
MODIS	Jul. HR	–	Phase 2	Phase 2	–
AOD = 0.14	Aug. MR	–	$+20° \Rightarrow -16h30$ arcmin	$+5° \Rightarrow -4h$	–
$\Delta AOD = 2.5 \times 10^{-3}$	Sep. MR	–	–	–	–
CF = 0.55	Oct. HR	–	–	–	–
$\Delta CF = 1.0 \times 10^{-3}$	Nov. HR	–	–	–	–
	Dec. MR	–	–	–	–

Tables 3, 5, 7, and 9 summarize the results calculated by the algorithm for the sites of Calern, Catania, Cebreros, and Lisbon, respectively.

In conclusion, the aerosol–cloud interaction algorithm described in this paper is user-friendly, works effectively with free available data, and does not require particular computational skills. It is versatile and exportable for all sites of scientific interest, and it estimates the relationship between aerosols and clouds applying a novel approach, demonstrating the fundamental importance of atmospheric particulate matter as a possible observational parameter to implement the forecasting models applicable to optical communication and astronomical observation in direct and predictive terms.

In future works, planned within the framework of the ESA funded ANAtOLIA project, the heterogeneity of the four analysed sites will be deepened to highlight the aspects in play in the aerosol–cloud interaction.

ACKNOWLEDGEMENTS

The Acknowledgments of the authors goes to the ANAtOLIA (Atmospheric monitoring to Assess the availability of Optical Links through the Atmosphere) ESA ITT AO/1-9936/17/UK/ND project funded by the European Space Agency, the Centre National d'Etudes Spatiales (CNES), and the Norwegian Space Agency.

MODIS and OMI data were provided by the *Giovanni – Interactive Visualization and Analysis* website. We thank the PI(s), Co-I(s), and their staff for establishing and maintaining the AERONET sites used in this investigation.

DATA AVAILABILITY

A part of the data underlying this paper will be shared on reasonable request to the corresponding author while a part of the data are available as described in the paper footnote.

REFERENCES

Ackerman A. S., Toon O. B., Hobbs P. V., 1994, Nature, 367, 445
Almeida G. P., 2023, Atmos. Environ., 295, 119517
Ammerlaan B. A. J., Holzinger R., Jedynska A. D., Henzing J. S., 2017, Atmos. Environ., 164, 1
Anwar K., Alam K., Liu Y., Huang Z., Huang J., Liu Y., 2022, Atmos. Res., 275, 106241
Aristidi E., Ziad A., Chabè J., Fantei-Caujolle Y., Renaud C., Giordano C., 2019, MNRAS, 486, 915
Aristidi E., Fantei-caujolle Y., Giordano C., Ziad A., Chabè J., 2022, in Schreiber L., Schmidt D., Vernet E., eds, Proc. SPIE Conf. Ser. Vol. 12185, Adaptive Optics Systems VIII. SPIE, Bellingham, p. 1218564
Bertolin C., Cavazzani S., 2022, Heliyon, 8, 11
Bosveld F. C., Baas P., Beljaars A. C. M., Holtslag A. M., de Arellano J. V., van de Wiel B. J. H., 2020, Bound.-Layer Meteorol., 177, 583
Cavazzani S., Zitelli V., 2013, MNRAS, 429, 1849
Cavazzani S., Ortolani S., Zitelli V., Maruccia Y., 2011, MNRAS, 411, 1271
Cavazzani S., Ortolani S., Zitelli V., 2012, MNRAS, 419, 3081
Cavazzani S., Rodeghiero G., Capraro I., Ortolani S., Barbieri C., Zitelli V., 2014, PASP, 126, 312
Cavazzani S., Ortolani S., Zitelli V., 2015, MNRAS, 452, 2185
Cavazzani S., Ortolani S., Zitelli V., 2017, MNRAS, 471, 2616
Cavazzani S., Ortolani S., Scafetta N., Zitelli V., Carraro G., 2019, MNRAS, 484, L136
Cavazzani S., Ortolani S., Bertolo A., Binotto R., Fiorentin P., Carraro G., Saviane I., Zitelli V., 2020a, MNRAS, 493, 2463
Cavazzani S., Ortolani S., Bertolo A., Binotto R., Fiorentin P., Carraro G., Zitelli V., 2020b, MNRAS, 499, 5075
Corsaro R. A. et al., 2017, J. Volcanol. Geotherm. Res., 341, 53
Dali Ali W. et al., 2010, A&A, 524, A73
Deshler T., 2003, Encycl. Atmos. Sci. Int. Geophys., 65, 129
Fernandez A. J., Apituley A., Veselovskii I., Suvorina A., Henzing J., Pujadas M., Artinano B., 2015, Atmos. Environ., 120, 484
Giordano C., Vernin J., Trinquet H., Munoz-Tunon C., 2014, MNRAS, 440, 1964
Giordano C., Rafalimanana A., Ziad A., Aristidi E., Chabè J., Fanteï-Caujole Y., Renaud C., 2021, MNRAS, 504, 1927
Kiran V. R. et al., 2022, Atmos. Meas. Tech., 15, 4709
Liu L. Y., Giordano C., Yao Y. Q., Vernin J., Chadid M., Wang H. S., Yin J., Wang Y. P., 2015, MNRAS, 451, 3299
Liu D., He C., Schwarz J. P., Wang X., 2020, NPJ Clim. Atmos., 3, 40
Loeb N., Schuster G., 2008, J. Geophys. Res. Atmos., 113, D14214
Magee R., Ubidea T., Caulfieldab J., 2021, Earth Planet. Sci. Lett., 565, 116904
Sahoo S., Tiwari D. K., Panda D., Kundu B., 2022, J. Geodyn., 149, 101896
Seiki T., Nakajima T., 2014, J. Atmos. Sci., 71, 833

Downloaded from https://academic.oup.com/rasti/article/2/1/420/7226210 by CNRS - ISTO user on 04 September 2023

Svensmark H., Enghoff M. B., Shaviv N. J., Svensmark J., 2017, Nat. Commun., 8, 2199
Taylor J. R., 1999, Introduction to Error Analysis (Texts and Manuals, Zanichelli). University Science Books, Herndon, VA
Ventura J. F., Russchenberg W. J., 2009, Phys. Chem. Earth, Parts A/B/C, 34, 88
Zeller J., Manzur T., 2010, in Carapezza E. M., ed., Proc. SPIE Conf. Ser. Vol. 7833, Unmanned/Unattended Sensors and Sensor Networks VII. SPIE, Bellingham, p. 7833
Ziad A. et al., 2022, in Schreiber L., Schmidt D., Vernet E., eds, Proc. SPIE Conf. Ser. Vol. 12185, Adaptive Optics Systems VIII. SPIE, Bellingham, p. 12185

This paper has been typeset from a TEX/LATEX file prepared by the author.

Downloaded from https://academic.oup.com/rasti/article/2/1/420/7226210 by CNRS - ISTO user on 04 September 2023

© 2023 The Author(s)
2023. Published by Oxford University Press on behalf of Royal Astronomical Society. This is an Open Access article distributed under the terms of the Creative Commons Attribution License (http://creativecommons.org/licenses/by/4.0/), which permits unrestricted reuse, distribution, and reproduction in any medium, provided the original work is properly cited.